Hindawi
International Journal of Aerospace Engineering
Volume 2023, Article ID 9948732, 13 pages
https://doi.org/10.1155/2023/9948732

Research Article

A Novel Active Vibration Control Method for Helicopter Fuselages Based on Diffusion Cooperation

Jingliang Li and Yang Lu

National Key Laboratory of Helicopter Aeromechanics, College of Aerospace Engineering, Nanjing University of Aeronautics and Astronautics, Nanjing 210016, China

Correspondence should be addressed to Yang Lu; luyang@nuaa.edu.cn

Received 10 December 2022; Revised 7 March 2023; Accepted 21 April 2023; Published 11 May 2023

Academic Editor: Tuo Han

Against the background of low-frequency vibration control for a helicopter fuselage in flight, active control of structural response (ACSR) has been employed for vibration control design. With the increase in control positions in the fuselage, more actuators and error sensors are needed to meet the vibration reduction requirements, forming a large-scale multichannel system. This leads to a rapid increase in the computation amount, causing the control performance of the conventional centralized algorithm main processor to become poor under overload operation. To this end, a novel distributed active vibration control algorithm based on the diffusion cooperative strategy was proposed and explored in this research. The diffusion cooperative strategy is widely used in complex wireless sensor network (WSN) systems to efficiently reduce the computation amount during data aggregation. This distributed algorithm utilizes the advantages of the diffusion-cooperative strategy to reduce the computation amount and coupling relationship of the secondary path in a large-scale multichannel system. First, a novel control law was established by introducing the network topology of the diffusion cooperation strategy into the classical filtered-x least mean square (FxLMS) algorithm, forming the diffusion FxLMS (DFxLMS) algorithm. Then, a secondary path trade-off quantization standard based on the complex undirected network connectivity condition was developed. It determined whether a secondary path was discarded or not and formed the topology of a large-scale multichannel system control network. To examine the effectiveness and superiority of the proposed DFxLMS algorithm, a comparative simulation with a scale of $1 \times 10 \times 10$ was carried out for a simplified helicopter fuselage. Numerical results in realistic scenarios showed the ability of the DFxLMS algorithms to achieve good control performance when proper values of these parameters are chosen.

1. Introduction

Helicopters are a kind of aircraft that can hover, take off, and land vertically. They play an irreplaceable roles in dealing with emergencies and disaster relief. However, severe low-frequency vibration of the fuselage, which can significantly reduce the comfort of pilots and passengers, has long been a difficult point and hot spot in the field of helicopter technology worldwide. As one of the most effective measures to reduce mechanical vibrations, active vibration control technology can overcome the poor effect of traditional passive measures at low frequencies [1]. In the active vibration control field, active control of structural response (ACSR) technology has been used to reduce the vibration of fuselages such as the W30, UH-60 M, EC225/EC725, and Z-11 [2–5], due to its advantages of better control performance, lightweight, strong frequency adaptability, etc.

The traditional ACSR system is relatively small because it only considers the vibration of some specific positions in the cockpit of the pilot and passenger. However, with the rapid development of high-speed helicopters, the vibrations of the dashboard, hub and tail boom have become new challenges for helicopter safety and airworthiness. For example, Sikorsky used an ACSR system with a scale of 10×6 to solve the fuselage vibration problem of X2 in high-speed forward flight [6]. With the increase in the number of actuators and error sensors, an ACSR system has more than 100 secondary paths, forming a large-scale multichannel system.

Assuming the numbers of reference sensors, error sensors, and actuators are all N, the computation amount of the simplest adaptive algorithm is proportional to N^4 [7, 8]. As a result, the centralized algorithm based on the main processor has poor control performance in the case of this huge computation burden [9].

A distributed algorithm based on multiprocessor cooperative operation is an effective way to reduce the computation amount and the coupling of secondary paths. Gao et al. [10] proposed a decentralized decoupling optimization control algorithm, which can effectively reduce the computation amount, but it was difficult to construct feedback compensation factors for a large-scale multichannel system. Zhang et al. [8] investigated a distributed multichannel adaptive algorithm for exploring the feasibility of error sensor signal decoupling. However, this algorithm does not weaken the coupling relationship of the secondary path. Ferrer et al. [11] presented a distributed algorithm with an incremental collaborative strategy, but their ring topology network is difficult to implement in many cases. Thus, the conventional distributed algorithm is not suitable for large-scale multichannel systems.

To this end, a novel distributed algorithm based on a diffusion cooperative strategy, a widely used method in the data aggregation algorithm of wireless sensor networks (WSNs) [12–14], is presented in this paper. This distributed algorithm utilized the advantages of a diffusion-cooperative strategy network topology to relieve the coupling of secondary paths and reduce the computation amount by discarding some secondary paths. For this purpose, we define a general control node as consisting of one error sensor and one actuator together with a unique processor with communication capabilities. In this research, the network topology of the diffusion cooperative strategy was combined with the filtered-x least mean square (FxLMS) algorithm because it has outstanding control performance in the active control of sound and vibration [15, 16], forming a diffusion FxLMS (DFxLMS). The DFxLMS algorithm only considers the secondary paths retained after quantization when updating the weight vector of the adaptive filter. This ensures convergence of the control system and significantly reduces the computation amount.

In summary, aiming at problems such as insufficient processor computing power and difficult hardware implementation when the centralized algorithm is used in a large-scale helicopter active vibration control system, the DFxLMS algorithm suitable for a large-scale multichannel system is proposed in this paper. Through theoretical analysis and simulation research, the contributions of this paper can be summarized as follows:

(1) The vibration acceleration response signal of each node decreased by more than 99.23% when compared with the uncontrolled response. In addition, the total computation amount was reduced by 22.86% when compared with the centralized algorithm

(2) The optimal convergence coefficient was slightly larger than that of the centralized algorithm, which is conducive to parameter selection and accelerated algorithm convergence

(3) Except for a few nodes, the stability control performance of the DFxLMS algorithm at other nodes was better than that of the centralized algorithm

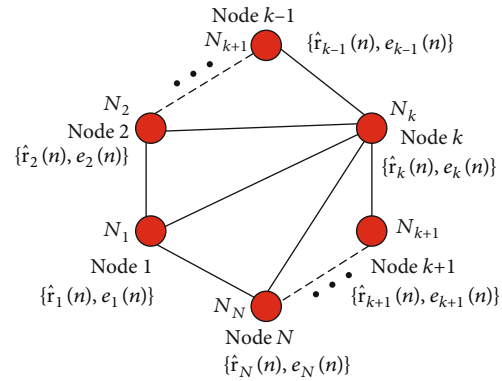

Figure 1: The topology network with N nodes.

This work is organized as follows. Section 2 gives the relevant contents of the novel method in detail. Section 3 carries out numerical simulations with and without the DFxLMS algorithm. Section 4 summarizes the numerical simulation results and draws valuable conclusions.

2. A Novel Method for Active Vibration Control

In this section, we describe the process of combining the network topology of the diffusion cooperative strategy with the FxLMS algorithm to form the DFxLMS algorithm. In particular, a secondary path trade-off quantization standard and its implementation process are depicted in detail. Moreover, the computation amount and stability are discussed to prove the superiority of the proposed method.

2.1. DFxLMS Algorithm. Assume that a large-scale multichannel system control network composed of N nodes is distributed in the helicopter fuselage. An undirected graph $G = (V, E)$ is used to represent the topology of this control network, where $V = \{1, 2, \cdots, N\}$ is the set of nodes and $E = \{(l, k) | l, k \in V\}$ is the set of edges. If and only if there is a nondiscarded secondary path between node k and node l satisfying $(l, k) \in E$, node k and node l are neighboring nodes. The set of nodes connected to node k (including k itself) is denoted by N_k. In graph theory, a graph G whose edges are indicated by arrows is called directed; otherwise, it is called undirected. In addition, an undirected graph G is connected if there is a path in G from every node to every other node; otherwise, it is unconnected [17–19]. The number of nodes connected to node k is called the degree of node k, and this is denoted by $|N_k|$. Figure 1 shows that the neighbor node set of node 1 is $N_1 = \{1, 2, k, N\}$, then $|N_1| = 4$.

In Figure 1, node k updates the weight vector of its adaptive filter by only using the secondary paths between its neighbor nodes. Discarding secondary paths can significantly reduce the computation amount of its processor and

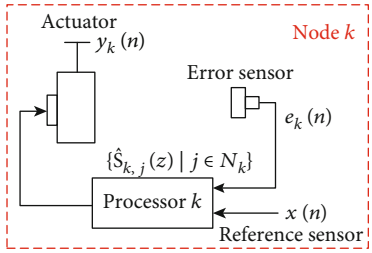

Figure 2: The structure of control node k.

is conducive to the selection of the convergence coefficient [20, 21]. Assume that a large-scale multichannel system has I reference sensors, J actuators, and J error sensors. Then, there are $I \times J$ primary paths and $J \times J$ secondary paths. It can be divided into J control nodes. The structure of control node k is shown in Figure 2. The block diagrams of the centralized algorithm and DFxLMS algorithm are depicted in Figure 3.

In Figure 3(a), MEFxLMS is short for multiple error filtered-x LMS. The most obvious difference between Figure 3(a) and Figure 3(b) is that the centralized algorithm adopts the main processor to realize active vibration control, while the DFxLMS algorithm is implemented based on multiprocessor cooperative control. In addition, the former considers all secondary paths, while the kth processor of the latter only uses the secondary paths determined by N_k.

The model of all neighboring secondary paths of the node k can be defined as $\{\hat{\mathbf{S}}_{k,j}(z) | j \in N_k\}$, and the filtered reference signal at node k is

$$\hat{r}_{k,j}(n) = \hat{\mathbf{S}}_{k,j}^{\mathrm{T}} \mathbf{x}_s(n), \tag{1}$$

where $\mathbf{x}_s(n) = [x(n), x(n-1), \cdots, x(n-L_s+1)]^{\mathrm{T}}$ and L_s is the order of the transverse filter.

The filtered reference signal is combined based on the control topology network

$$\hat{\mathbf{r}}_k(n) = \left[a_{1,k}\hat{\mathbf{r}}_{k,1}^{\mathrm{T}}(n), \cdots, a_{j,k}\hat{\mathbf{r}}_{k,j}^{\mathrm{T}}(n), \cdots, a_{J,k}\hat{\mathbf{r}}_{k,J}^{\mathrm{T}}(n)\right]^{\mathrm{T}}, \tag{2}$$

where $\hat{\mathbf{r}}_{k,j}(n) = [\hat{r}_{k,j}(n), \hat{r}_{k,j}(n-1), \cdots, \hat{r}_{k,j}(n-L+1)]^{\mathrm{T}}$, L is the adaptive filter order, and the combining coefficient $\{a_{j,k} \geq 0\}$ is determined by the retained secondary paths.

The error signal is defined as

$$\mathbf{e}(n) = \mathbf{d}(n) - \hat{\mathbf{R}}^{\mathrm{T}}(n)\mathbf{W}(n), \tag{3}$$

where $\mathbf{W}(n)$ is the estimated value of the optimal solution $\mathbf{W}^{\mathrm{o}} \in \mathrm{R}^{LJ}$ of the adaptive filter of the control network at time n, and

$$\begin{aligned}
\hat{\mathbf{R}}(n) &= \left[\hat{\mathbf{R}}_1(n), \hat{\mathbf{R}}_2(n), \cdots, \hat{\mathbf{R}}_J(n)\right], \\
\mathbf{e}(n) &= \left[e_1(n), e_2(n), \cdots, e_J(n)\right]^{\mathrm{T}}, \\
\mathbf{d}(n) &= \left[d_1(n), d_2(n), \cdots, d_J(n)\right]^{\mathrm{T}}, \\
\hat{\mathbf{R}}_k(n) &= \left[\hat{\mathbf{r}}_{k,1}^{\mathrm{T}}(n), \hat{\mathbf{r}}_{k,2}^{\mathrm{T}}(n), \cdots, \hat{\mathbf{r}}_{k,J}^{\mathrm{T}}(n)\right]^{\mathrm{T}}.
\end{aligned} \tag{4}$$

The actuator force of node k is

$$y_k(n) = \mathbf{w}_k^{\mathrm{T}}(n)\mathbf{x}(n), \tag{5}$$

where $\mathbf{w}_k(n) = [\mathbf{W}(n)]_{L(k-1)+1:Lk}$ and $\mathbf{x}(n) = [x(n), x(n-1), \cdots, x(n-L+1)]^{\mathrm{T}}$. The total actuator force is $\mathbf{y}(n) = [y_1(n), y_2(n), \cdots, y_J(n)]^{\mathrm{T}}$.

With the filtered reference signal, the weight vector of the global adaptive filter can be updated iteratively. The weight vector update equation is defined as

$$\mathbf{W}(n+1) = \mathbf{W}(n) + \mu\hat{\mathbf{r}}(n)\mathbf{e}(n), \tag{6}$$

where $\hat{\mathbf{r}}(n) = [\hat{\mathbf{r}}_1(n), \hat{\mathbf{r}}_2(n), \cdots, \hat{\mathbf{r}}_J(n)]$ and μ is the convergence coefficient determined by the convergence condition.

2.2. Secondary Path Trade-off Quantization Standard. From Equation (2), we see that the combination coefficient $\{a_{j,k} \geq 0\}$ is very important for the DFxLMS algorithm. Its value is determined by the secondary paths retained after quantization. In other words, it contains the topology information of the control network. A diffusion cooperation strategy was applied to the data aggregation algorithm in the WSN to solve the problems of data redundancy and wireless communication congestion caused by the rapid increase in the number of sensors in the monitored environment [12–14]. In a WSN, the communication between different nodes depends on the node distance [22]. Similarly, the relative magnitude of the output signal amplitude of each secondary path in the active vibration control system represents the degree of the coupling relationship. First, a quantization threshold is set. The secondary path will be discarded when its output signal amplitude is lower than the quantization threshold. Then, the nondiscarded secondary path represents the edge in the topology of the control network. Thus, a secondary path trade-off quantization standard was designed, which discarded some secondary paths to reduce the computation amount and relieved the coupling relationship of the secondary path in the large-scale multichannel active vibration control system of the helicopter fuselage.

Algorithm 1 summarizes the implementation process of the secondary path trade-off quantization standard in the DFxLMS algorithm. This process is repeated until the combination matrix A just meets the complex undirected network connectivity [23, 24]. At this point, the reduction in computation is the most obvious. Therefore, this value is the optimal quantization threshold.

The topology connectivity of the large-scale multichannel system control network composed of J nodes is visually expressed in Figure 4. Some nodes have no reachable path

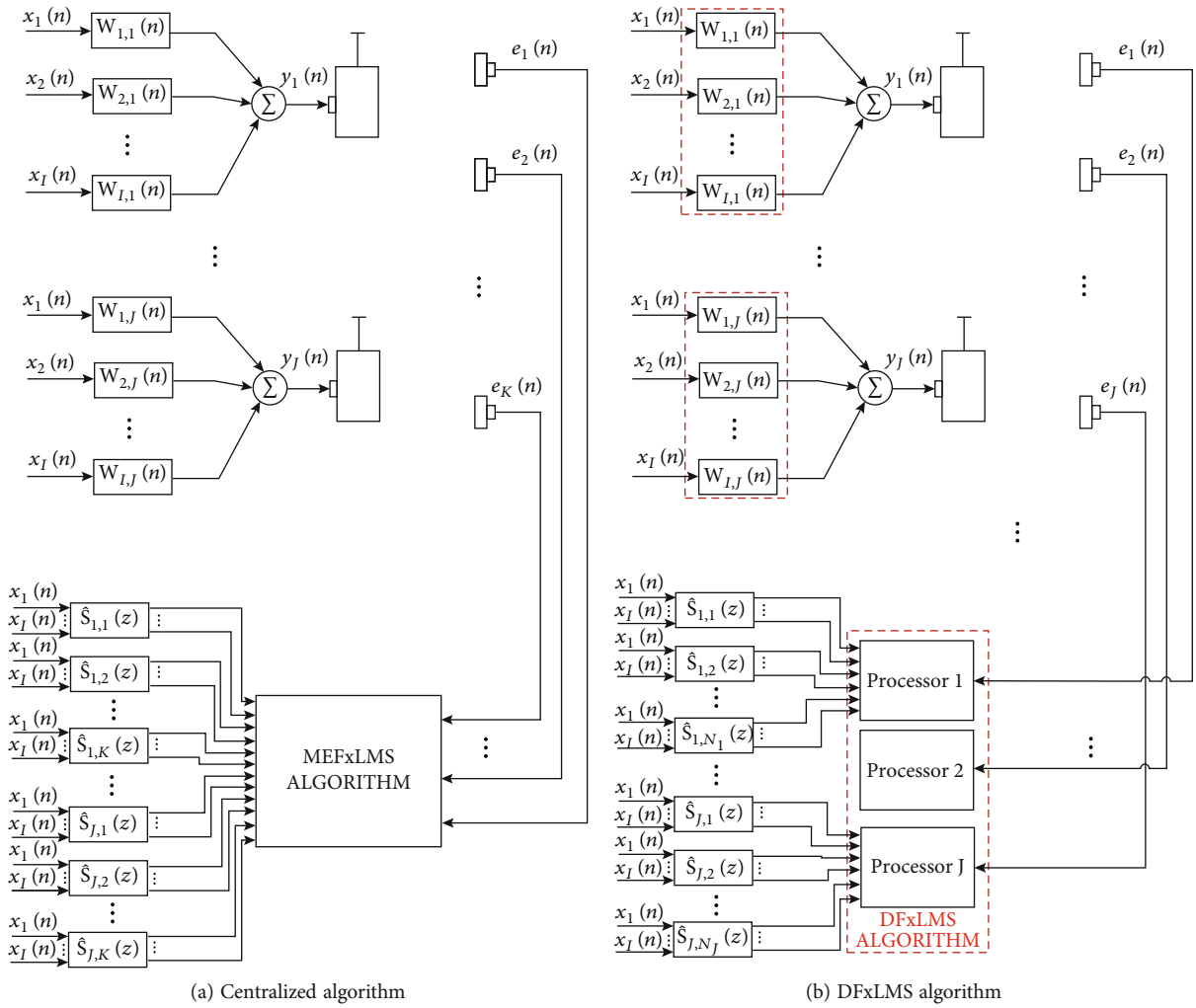

(a) Centralized algorithm (b) DFxLMS algorithm

FIGURE 3: Block diagrams of the centralized algorithm and DFxLMS algorithm.

Steps

1) actuator 1 action, response amplitudes $[c_{11}, c_{12}, \cdots, c_{1k}, \cdots, c_{1J}]$
2) actuator 2 action, response amplitudes $[c_{21}, c_{22}, \cdots, c_{2k}, \cdots, c_{2J}]$
3) actuator J action, response amplitudes $[c_{J1}, c_{J2}, \cdots, c_{Jk}, \cdots, c_{JJ}]$
4) response amplitude matrix C
5) quantization threshold is $b(0<b<1)$
6) for i=1:length (C)
    for j=1:length (C)
        if $(C(i,j) < b * \max(C,[],2))$
            $A(i,j)=0$;
        else
            $A(i,j) =1$;
        end
    end
end
7) combination matrix $A=A+A^{T}+I$

ALGORITHM 1: Steps of secondary path trade-off quantization standard.

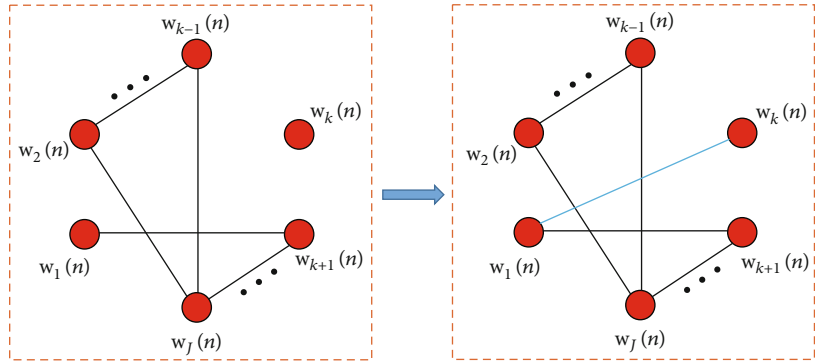

(a) Disconnected network (b) Connected network

Figure 4: The topology connectivity of the large-scale system control network.

Table 1: Computation amount of the DFxLMS algorithm.

Steps	Computing formula	Computation
1	$\hat{\mathbf{r}}_k(n) = \left[a_{1,k}\hat{\mathbf{r}}_{k,1}^{\mathrm{T}}(n),\cdots,a_{j,k}\hat{\mathbf{r}}_{k,j}^{\mathrm{T}}(n),\cdots,a_{J,k}\hat{\mathbf{r}}_{k,J}^{\mathrm{T}}(n)\right]^{\mathrm{T}}$	$\sum_{k=1}^{J}\lvert N_k\rvert IL_s$
2	$\hat{\mathbf{r}}(n) = \left[\hat{\mathbf{r}}_1(n),\hat{\mathbf{r}}_2(n),\cdots,\hat{\mathbf{r}}_J(n)\right]$ $\mathbf{W}(n+1) = \mathbf{W}(n) + \mu\hat{\mathbf{r}}(n)\mathbf{e}(n)$	IJ^2L
3	$y_k(n) = \mathbf{w}_k^{\mathrm{T}}(n)\mathbf{x}(n)$	IJL

in Figure 4(a), and all nodes have a path from every node to every other node in Figure 4(b).

2.3. Discussion of Computation Amount. To quantitatively illustrate the advantages of the DFxLMS algorithm in reducing the computation amount when applied to a large-scale multichannel system, the amounts of computation required by the DFxLMS algorithm for each step of one control cycle are shown in Table 1.

Then, the computation amount required by the DFxLMS algorithm for one cycle is

$$N_{\mathrm{DFxLMS}} = \sum_{k=1}^{J}|N_k|IL_s + (J+1)IJL. \tag{7}$$

The centralized algorithm computation amount for one cycle is [25]

$$N_{\mathrm{MIMO}} = IJ^2(L+L_s) + IJL. \tag{8}$$

Variable $|N_k|$ represents the number of secondary paths retained by node k, and its value ranges from 1 to J. When all nodes are set to 1, this means that the control network only retains the paired secondary paths within the nodes, so the DFxLMS algorithm degenerates into the traditional distributed algorithm. When all nodes are set to J, the control network retains all secondary paths, which does not help reduce the computation amount or relieve the coupling of the secondary path.

2.4. Discussion of Stability Condition. Equation (6) shows that the convergence coefficient μ is crucial to updating the weight vector of the global adaptive filter. A smaller value can ensure the convergence of the update process, but the convergence process is slow. Although a larger value can increase the convergence speed, this may cause divergence in the update process. Therefore, it is necessary to analyze the stability of the DFxLMS algorithm to obtain the convergence condition and provide a theoretical foundation for the value of the convergence coefficient μ.

The global Lyapunov function is

$$V(n) = \sum_{k=1}^{K}V_k(n) = \sum_{k=1}^{K}\frac{1}{2}{e_k}^2(n). \tag{9}$$

At node k, the differential form can be expressed as

$$\begin{aligned}\Delta V_k(n) &= V_k(n+1) - V_k(n) = \frac{1}{2}\left[{e_k}^2(n+1) - {e_k}^2(n)\right]\\ &= \frac{1}{2}[e_k(n+1) - e_k(n)][e_k(n+1) + e_k(n)]\\ &= \frac{1}{2}\Delta e_k(n)[2e_k(n) + \Delta e_k(n)].\end{aligned} \tag{10}$$

Theoretically, $\Delta e_k(n)$ can be further expressed as

$$\begin{aligned}\Delta e_k(n) &= e_k(n+1) - e_k(n) = \left[\frac{\partial e_k(n)}{\partial \mathbf{W}(n)}\right][\Delta\mathbf{W}(n)]\\ &= -\hat{\mathbf{R}}_k^{\mathrm{T}}(n)[\mu_k e_k(n)\hat{\mathbf{r}}_k(n)] = -\mu_k e_k(n)\hat{\mathbf{R}}_k^{\mathrm{T}}(n)\hat{\mathbf{r}}_k(n).\end{aligned} \tag{11}$$

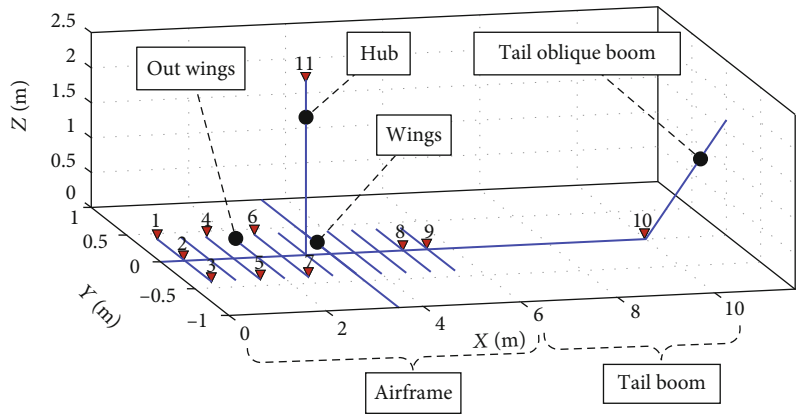

Figure 5: Numerical simulation model and $1 \times 10 \times 10$ large-scale multichannel system.

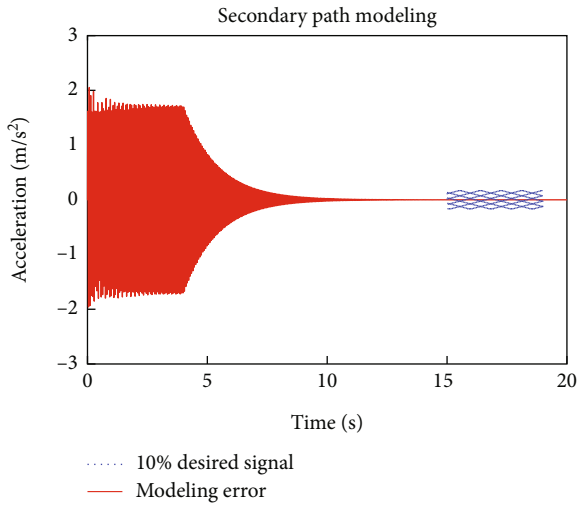

Figure 6: Secondary path modeling of $S_{6,1}(z)$.

Substituting Equation (11) into Equation (10), we can obtain

$$\begin{aligned}\Delta V_k(n) &= \frac{1}{2}\left[-\mu_k e_k(n)\hat{\mathbf{R}}_k^{\mathrm{T}}(n)\hat{\mathbf{r}}_k(n)\right] \\ &\quad \cdot \left[2e_k(n) - \mu_k e_k(n)\hat{\mathbf{R}}_k^{\mathrm{T}}(n)\hat{\mathbf{r}}_k(n)\right] \\ &= -\frac{1}{2}\mu_k {e_k}^2(n)\hat{\mathbf{R}}_k^{\mathrm{T}}(n)\hat{\mathbf{r}}_k(n)\left[2 - \mu_k \hat{\mathbf{R}}_k^{\mathrm{T}}(n)\hat{\mathbf{r}}_k(n)\right].\end{aligned} \tag{12}$$

From Eq. (9), the global Lyapunov function $V(n) = \sum_{k=1}^{K} V_k(n) = \sum_{k=1}^{K} 1/2{e_k}^2(n) \geq 0$, if and only if $e_k(n) = 0$, then $V(n) = 0$. According to the Lyapunov theorem, when $\Delta V_k(n) \leq 0$, the control system is stable and generally requires $\Delta V_k(n) < 0$; then,

$$2 - \mu_k \hat{\mathbf{R}}_k^{\mathrm{T}}(n)\hat{\mathbf{r}}_k(n) > 0. \tag{13}$$

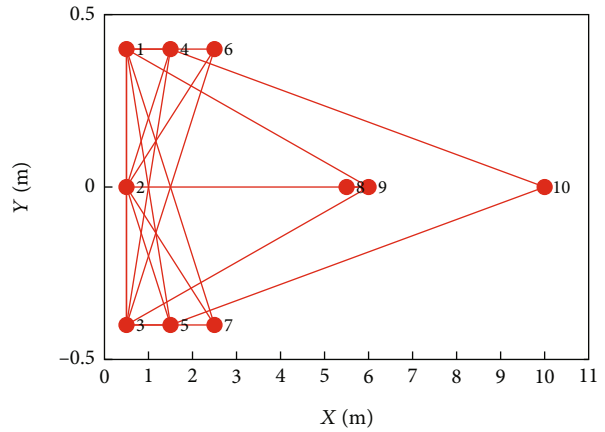

Figure 7: Topology network with a quantization threshold of 88%.

The value range of the convergence coefficient of node k can be obtained from the above formula

$$0 < \mu_k < \frac{2}{\hat{\mathbf{R}}_k^{\mathrm{T}}(n)\hat{\mathbf{r}}_k(n)}. \tag{14}$$

It should be noted that the influence of the combination coefficient $\{a_{j,k}\}$ on algorithm stability is reflected in $\hat{\mathbf{r}}_k(n)$. When the convergence coefficients of each node all meet the value range, the weight vector of the adaptive filter based on the DFxLMS algorithm converges to the optimal solution $\mathbf{W}^{\mathrm{o}}$. In the numerical simulations, a certain optimization method is used to constantly adjust the convergence coefficient to make the DFxLMS algorithm converge at the fastest speed.

3. Numerical Simulations

To verify the effectiveness and superiority of the DFxLMS algorithm for a large-scale multichannel system, a simplified helicopter fuselage model was used to conduct vibration suppression simulation with a system scale of $1 \times 10 \times 10$.

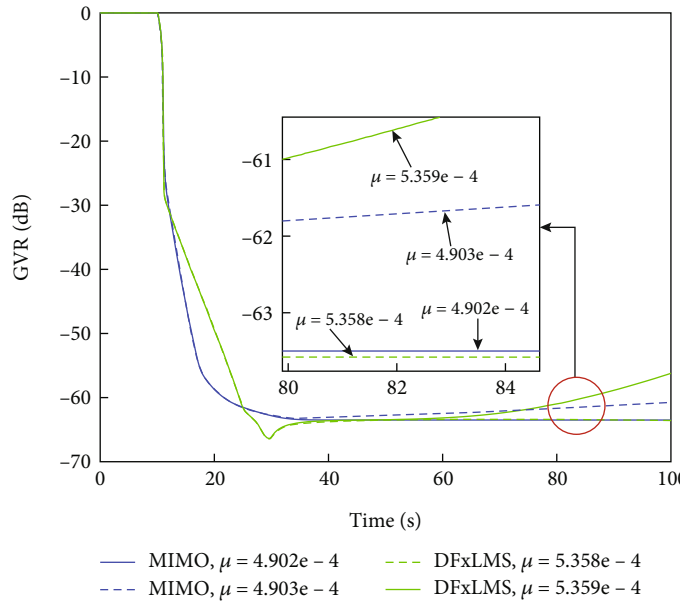

Figure 8: Control performances of different convergence coefficients.

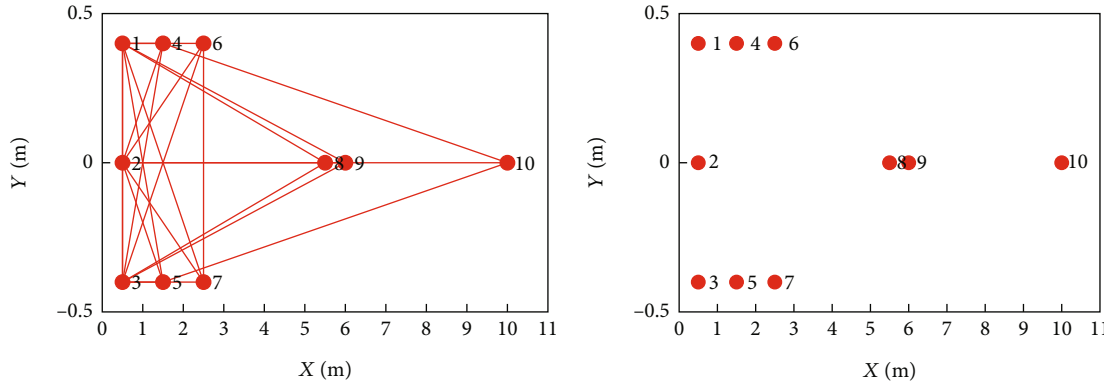

Figure 9: Topology network with different quantization thresholds.

3.1. Simulation Model. The numerical simulation model and $1 \times 10 \times 10$ large-scale multichannel system are shown in Figure 5. This model weight is 6.1×103 kg and is composed of an airframe, tail boom, wings, tail oblique boom, outer wings, and hub. Nodes 1-10 are the feedback signal positions, which are distributed in the instrument panel, pilot's seats, passenger's seats, and tail boom [26, 27]. Node 11 is the disturbance signal position of the main rotor. As mentioned above, this $1 \times 10 \times 10$ large-scale multichannel system can be divided into 10 control nodes.

3.2. Secondary Path Modeling. The secondary path in the ACSR system has an important influence on the control performance, so the modeling accuracy of the secondary path can directly affect the stability and effectiveness of the control algorithm to a great extent [28, 29]. In time-domain control algorithms, the transverse filter is often used to estimate the secondary path [30]. There are two methods to model the secondary paths: offline and online [31, 32]. Since the characteristics of the secondary path in the active vibration control process of helicopter fuselages generally remain steady state, an offline modeling method can be adopted to simplify the control algorithm.

The transverse filter order L_s is 64, the initial value is set to 0, the sampling frequency of the adaptive modeling algorithm is 1000 Hz, and the modeling time is 20 s. To obtain a perfect secondary path for numerical simulation, the modeling error must be restrained to be within 10% of the desired signal. Figure 6 shows the modeling process of the secondary path $S_{6,1}(z)$. The blue dotted line indicates the 10% value of the desired signal, and the red solid line is the modeling error. As shown in Figure 6, the secondary path $S_{6,1}(z)$ modeling meets the requirements. For the large-scale multichannel system in this paper's simulation model, the total number of secondary paths is $10 \times 10 = 100$.

3.3. Simulation Results and Discussion. The DFxLMS algorithm simulation was carried out on a computer simulation

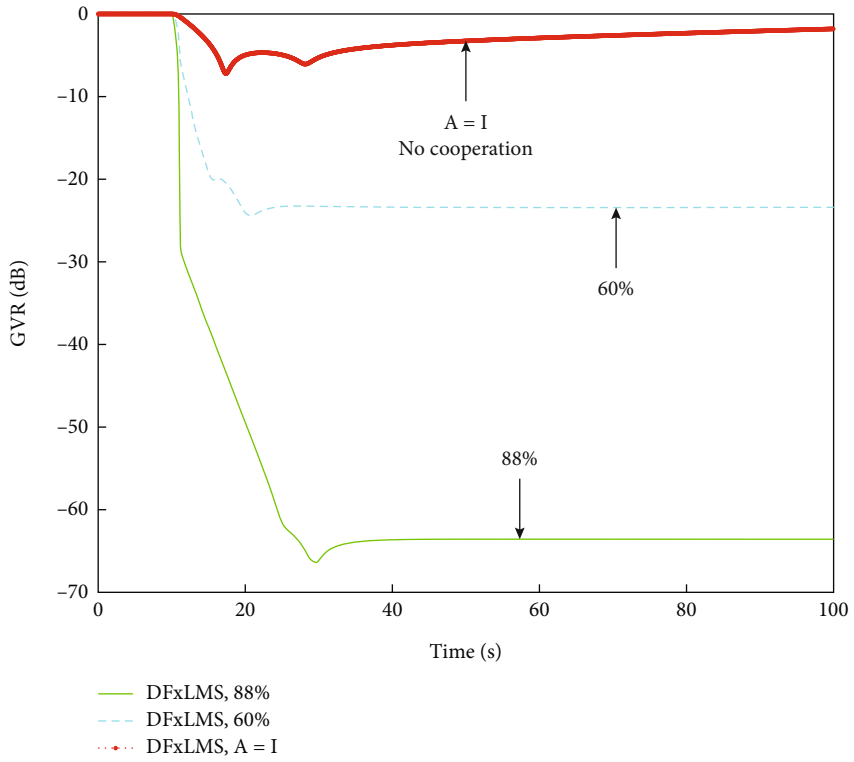

Figure 10: Control performances of the different quantization thresholds.

platform. The control performance of each node can be obtained from Equation (15), and the global control performance can be obtained from Equation (16).

$$VR_k(n) = 10 \lg \left\{ \frac{\sum e_k^2(n)}{\sum d_k^2(n)} \right\}, \tag{15}$$

$$GVR(n) = \frac{1}{J} \sum_{k=1}^{J} VR_k(n). \tag{16}$$

3.3.1. Selection of the Convergence Coefficient. Equation (6) shows that the value of the convergence coefficient μ is crucial to the weight vector updating process of the global adaptive filter. In this section, a traversal method is adopted to determine its optimal value.

When all the rotor blades are identical in size and weight, the resulting vibration is dominated by harmonic multiples ($p = 1, 2, 3, \cdots$) of the number of blades (N) multiplied by the main rotor speed (Ω). Helicopter fuselage vibration is primarily characterized by harmonic excitations from the main rotor at the first multiple, often referred to as $N\Omega$ [33–35]. To simulate the vibration state of the reference helicopter forward flying at 250 km/h, a harmonic disturbance force with a base frequency ($N\Omega$) of 17 Hz and amplitude of 4000 N was applied to node 11. The reference signal $x(n)$ was taken to be the same as the disturbance force [36, 37]. The expected signal $d(n)$ was the acceleration response of each control node without active control. The adaptive filter order L is 64, the initial value is set to 0, the sampling frequency is 1000 Hz, and the simulation duration is 100 s. Active control was applied after external disturbance excitation for 10 s. The quantization threshold of the secondary path was 88%, which was the upper limit to ensure the connectivity of the control network. The global control performance of Equation (16) is adopted as the evaluation index. Figure 7 shows the control topology network at this moment.

The convergence coefficient μ was first taken as a small value satisfying Equation (14), and then the convergence trend of the global control performance curve in the simulation was observed. A large step was adopted to gradually increase the convergence coefficient when the curve converged slowly and there was no stable state. In contrast, a small step was adopted. The iterative convergence coefficient to make the global control performance curve close to the fastest convergence speed was the optimal convergence coefficient. The simulation results of the global control performance curve of the optimal value and its slightly larger value with the DFxLMS algorithm and centralized algorithm are depicted in Figure 8. The MIMO in the legend represents the centralized algorithm.

In Figure 8, it is revealed that the DFxLMS algorithm achieved the same global control performance as the centralized algorithm with the stable vibration reduction amount reaching more than 62.8 dB. The divergence trend appears in the global control performance curves of the two algorithms when the convergence coefficient was slightly greater than the optimal value, and the divergence speed of the DFxLMS algorithm was obviously faster than that of the centralized algorithm. By comparing these four curves, the convergence value of the DFxLMS algorithm at the optimal

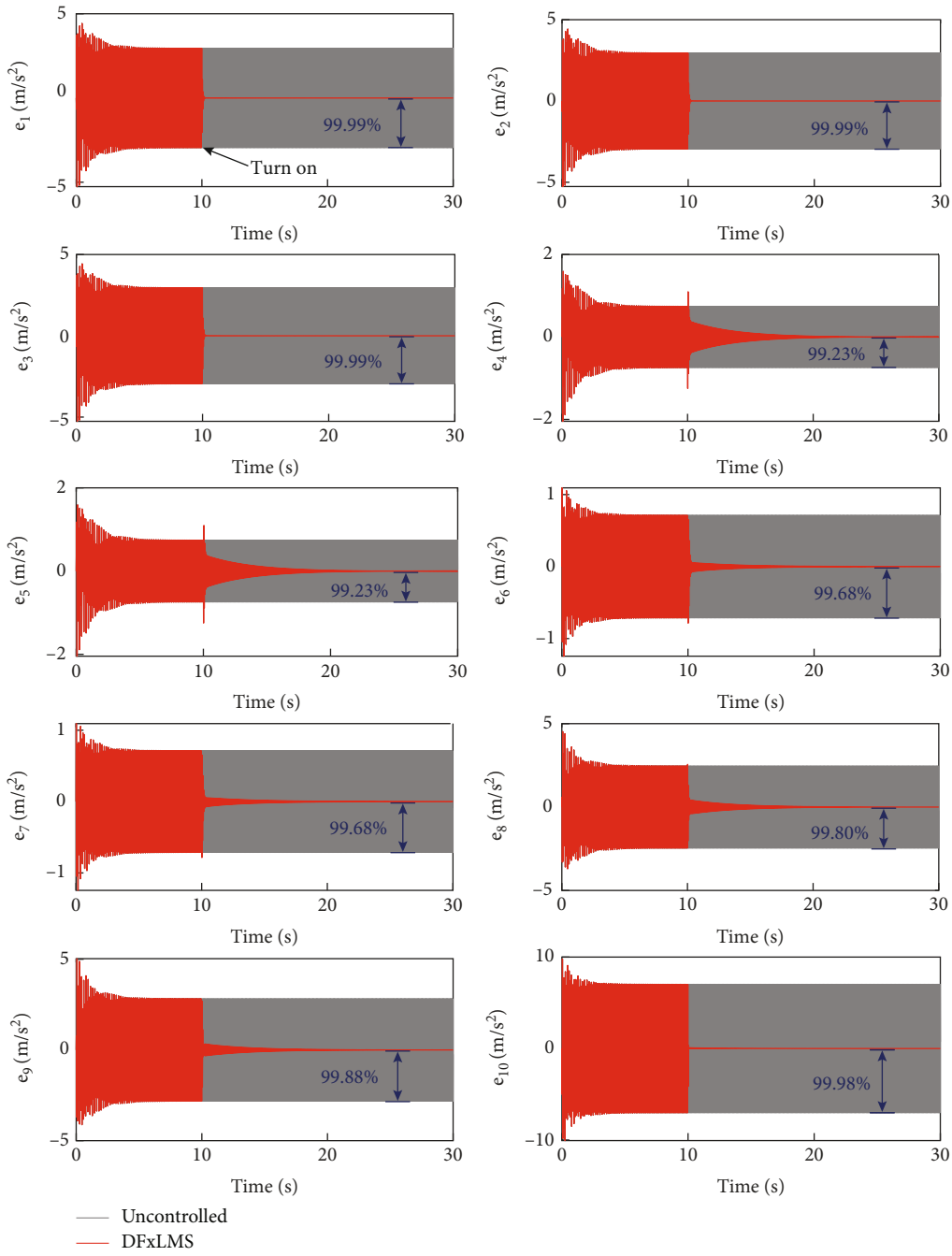

Figure 11: Acceleration response signals at the controlled nodes.

value ($\mu = 5.358e-4$) is seen to be slightly larger than that of the centralized algorithm ($\mu = 4.902e-4$). This was probably because the DFxLMS algorithm discarded some secondary paths with weak coupling relationships.

3.3.2. Quantization Threshold Setting. The influence of the combination coefficient $\{a_{j,k}\}$ on the stability of the algorithm is reflected in $\hat{\mathbf{r}}_k(n)$, which is an important part of Equation (14). Therefore, the optimal convergence coefficients corresponding to different quantization thresholds are usually different. To verify the feasibility and effectiveness of the secondary path quantization standard proposed in this paper, different quantization thresholds were set for comparative simulation. This needs to consider all secondary paths the same as the centralized algorithm when the quantization threshold is set to 0, resulting in difficulty in reducing the computation amount and relieving the secondary path coupling.

The traversal method process for finding the optimal quantization threshold is as follows. First, the initial quantization threshold is set at 100%, but the control network is disconnected at this time. Then, the quantization threshold is slowly reduced in steps of 1%. When the control network is just connected, this percentage value is the upper limit of

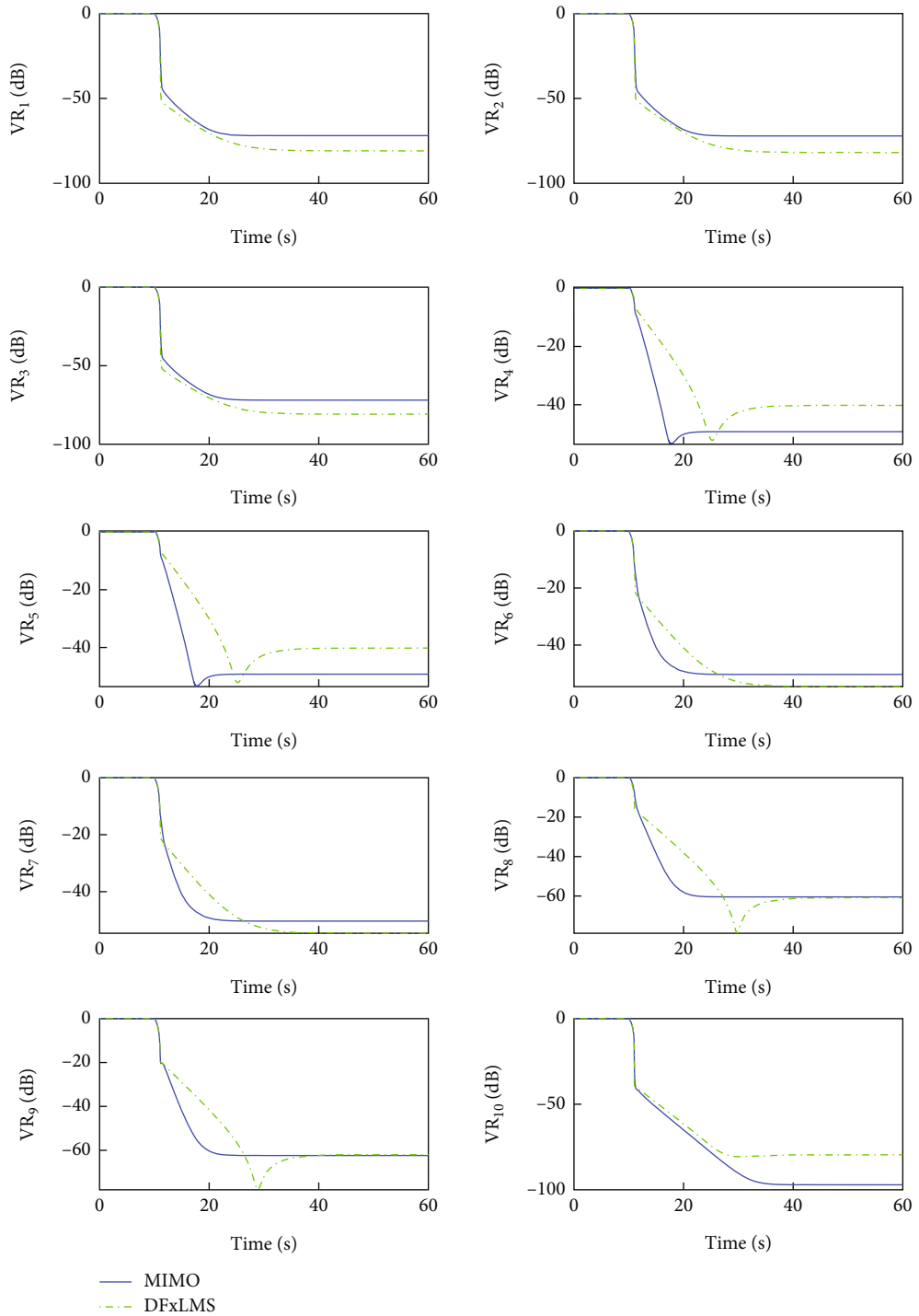

Figure 12: The control performances compared with the centralized algorithm.

the quantization threshold. Through this process, it can be obtained that the upper limit of the quantization threshold in this research was 88%. In addition, further reducing the quantization threshold means that more secondary paths need to be considered, which is unhelpful for reducing the computation amount and relieving the secondary path coupling.

This section only gives the simulation results when the quantization threshold values were 88%, 60%, and the identity matrix, respectively. Then, the corresponding optimal convergence coefficient also adopts the traversal method. It is worth mentioning that the identity matrix is called the no cooperation of the DFxLMS algorithm, which was also named the decentralized algorithm. The topological structure of the control network with a quantization threshold of 88% is shown in Figure 7, and the other two combination matrices of the control network are depicted in Figure 9. The global control performance curves are depicted in Figure 10.

Comparing the results of the three quantization thresholds, the thin solid line with a representative quantization threshold of 88% had the best control performance, and the stable global control performance was close to -62.8 dB. The dotted line control performance with the quantization threshold of 60% was the second best, and the global control performance was close to -23.1 dB. The thick solid line representing the identity matrix had the worst control performance, and the minimum global control performance was only -6.7 dB, and it was unstable.

Therefore, when the connectivity of the complex control network was satisfied, further reducing the quantization threshold degraded the control performance, by approximately 39.7 dB. This was because retaining too many secondary paths makes it difficult for the convergence coefficient to take the optimal value. The control performance of the no cooperation scenario was divergent on account of simply ignoring the coupling relationship of all secondary paths.

3.3.3. Based Frequency Control. According to the simulation results presented in the above two sections, the control performance was the best when the convergence coefficient was $\mu = 5.358e-4$ and the quantization threshold of the secondary path was 88%. To examine the effectiveness and superiority of the proposed DFxLMS algorithm, comparative simulations were performed with and without active vibration control. The simulation durations were 30 s. The external disturbance condition and other simulation parameters were the same as those used in the previous sections. Figure 11 shows the measured acceleration response signal in the time domain at each node with and without active vibration control.

It can be seen in Figure 11 that the vibration acceleration response signals were reduced by over 99.23% by using active control with the DFxLMS algorithm. At this time, the computation amount required for one control cycle of the centralized algorithm obtained from Equation (8) was 13440, while the DFxLMS algorithm computation was 10368 by substituting $\sum_{k=1}^{10}|N_k| = 52$ into Equation (7). Therefore, the DFxLMS algorithm can obtain the additional effect of a computation amount reduction of 22.86%.

Figure 8 shows that the global control effect of the diffusion algorithm was basically consistent with that of the centralized algorithm. To fully compare which of the two algorithms was superior, Figure 12 shows the comparison diagram of the control performances of the two algorithms at each node.

The convergence rates of curves VR_4 and VR_5 were quite different, while those of the other nodes were almost the same as the centralized algorithm before -20 dB. Except for VR_4, VR_5, and VR_{10}, the stable control performances of the DFxLMS algorithm were all better than those of the centralized algorithm.

4. Conclusions

In this paper, a novel distributed active control algorithm based on the diffusion cooperative strategy for reducing the huge computation amount and relieving the complex coupling of secondary paths in a large-scale multichannel system of helicopter fuselage was presented. The following conclusions describe the results of the previous sections.

(1) The DFxLMS algorithm reduced the computation amount by discarding some of the secondary paths while ensuring that the convergence of the ACSR system through nondiscarded secondary paths meets the complex undirected network connectivity

(2) The optimal convergence coefficient of the DFxLMS algorithm was slightly larger than that of the centralized algorithm

(3) The DFxLMS algorithm had the best control performance and the lowest computation amount when the quantization threshold just meets the control network connectivity

(4) In the frequency control simulation, the DFxLMS algorithm achieved outstanding control performance. The vibration acceleration response signals of all control nodes were reduced by over 99.23% when compared with the uncontrolled responses. Moreover, the computation amount was reduced by 22.86% when compared with the centralized algorithm. This verified the effectiveness and superiority of the proposed DFxLMS algorithm

Data Availability

The data supporting the findings of the study cannot be shared at this time as the data also form part of an ongoing study.

Conflicts of Interest

The authors declare that there is no conflict of interest regarding the publication of this article.

Authors' Contributions

All listed authors have made a significant scientific contribution to the research in the manuscript and agreed to be an author.

Acknowledgments

This work was supported by the Priority Academic Program Development of Jiangsu Higher Education Institutions (PAPD) and Nanjing University of Aeronautics and Astronautics Research and Practice Innovation Program (grant number xcxjh20210105). In this article, the authors acknowledge the help of Jiaming Sun for the theoretical analysis.

References

[1] C. Song, Y. Xiao, C. Yu, W. Xu, and J. Zhang, "H∞ active control of frequency-varying disturbances in a main engine on the

floating raft vibration isolation system," *Journal of Low Frequency Noise, Vibration and Active Control*, vol. 37, no. 2, pp. 199–215, 2018.

[2] S. P. King and A. E. Staple, *Minimization of helicopter vibration through active control of structural response*, Rotorcraft Design for Operations, AGARD-CP-423, 1986.

[3] T. A. Millott, R. K. Goodman, J. K. Wong, W. A. Welsh, J. R. Correia, and C. E. Cassil, "Risk reduction flight test of a preproduction active vibration control system for the UH-60M," in *Proceedings of the American Helicopter Society 59th Annual Forum*, Phoenix, Ariz, USA, 2003.

[4] B. Vignal and T. Krysinski, "Development and qualification of active vibration control system for the Eurocopter EC225/EC725," in *Proceedings of the 61st Annual Forum Proceedings AHS International*, Grapevibe, Tex, USA, 2005.

[5] Y. Lu, Z. Q. Gu, A. M. Ling, and M. Q. Li, "Flight test of active control of structure response for helicopter," *Journal of Vibration Engineering*, vol. 25, pp. 24–29, 2012.

[6] R. Blackwell and T. Millott, "Dynamic design characteristics of the Sikorsky X2 technology demonstrator aircraft," in *Proceedings of the 64th Forum of the American Helicopter Society*, Montreal, Canada, 2008.

[7] M. Glugla and R. K. Schulz, "Active vibration control using delay compensated LMS algorithm by modified gradients," *Journal of Low Frequency Noise, Vibration and Active Control*, vol. 27, no. 1, pp. 65–74, 2008.

[8] Q. Zhang, X. Yu, L. Yang, and H. Wu, "Research on distributed multi-channel active vibration isolation control algorithm," *Ship Engineering*, vol. 42, pp. 78–83, 2020.

[9] J. M. Song and P. G. Park, "A diffusion strategy for the multichannel active noise control system in distributed network," in *2016 International Conference on Computational Science and Computational Intelligence (CSCI)*, Las Vegas, NV, USA, 2017.

[10] W. Gao, G. He, L. Yang, and S. Liu, "Decentralized adaptive active vibration isolation control algorithm," *Journal of Vibration and Shock*, vol. 39, pp. 254–259, 2020.

[11] M. Ferrer, M. de Diego, G. Piñero, and A. Gonzalez, "Active noise control over adaptive distributed networks," *Signal Processing*, vol. 107, pp. 82–95, 2015.

[12] F. S. Cattivelli and A. H. Sayed, "Diffusion LMS strategies for distributed estimation," *IEEE Transactions on Signal Processing*, vol. 58, no. 3, pp. 1035–1048, 2010.

[13] C. G. Lopes and A. H. Sayed, "Diffusion least-mean squares over adaptive networks formulation and performance analysis," *IEEE Transactions on Signal Processing*, vol. 56, no. 7, pp. 3122–3136, 2008.

[14] F. S. Cattivelli, C. G. Lopes, and A. H. Sayed, "Diffusion recursive least-squares for distributed estimation over adaptive networks," *IEEE Transactions on Signal Processing*, vol. 56, no. 5, pp. 1865–1877, 2008.

[15] X. Ma, Y. Lu, and F. Wang, "Active structural acoustic control of helicopter interior multifrequency noise using input-output-based hybrid control," *Journal of Sound and Vibration*, vol. 405, pp. 187–207, 2017.

[16] S. Elliott, I. Stothers, and P. Nelson, "A multiple error LMS algorithm and its application to the active control of sound and vibration," *IEEE Transactions on Acoustics, Speech, and Signal Processing*, vol. 35, no. 10, pp. 1423–1434, 1987.

[17] C. Vasudev, "Graph theory with applications," *The Mathematical Gazette*, vol. 62, pp. 237-238, 2006.

[18] S. S. Ray, "Graph theory with algorithms and its applications," in *Applied Science and Technology*, Springer, India, 2013.

[19] Z. M. Hong, *Research on the eigenvalues and connectivity of graphs*, Economic Science Press, China: Beijing, 2022.

[20] F. Y. An, H. L. Sun, X. D. Li, and J. Tian, "Optimization of parameters in decentralized adaptive active control algorithm," *Journal of Vibration Engineering*, vol. 26, pp. 48–54, 2013.

[21] F. An, Y. Cao, and B. Liu, "Optimized decentralized adaptive control of noise and vibration for periodic disturbances," *Journal of the Acoustical Society of America*, vol. 144, no. 4, pp. -EL275–EL280, 2018.

[22] W. X. Chen, G. Y. Lu, and Q. D. Huang, "An improved distributed diffusion sign-LMS algorithm," *Telecommunication Engineering*, vol. 53, pp. 1580–1585, 2013.

[23] T. Z. Tan, S. X. Gao, and W. G. Yang, "Determining the connectedness of an undirected graph," *Journal of University of Chinese Academy of Sciences*, vol. 35, pp. 582–588, 2018.

[24] Z. Wang, B. Qin, Y. Xu, R. Lu, and Q. Wei, "An efficient algorithm for determining the connectivity of complex undirected networks," *Acta Automatica Sinica*, vol. 46, pp. 2129–2136, 2020.

[25] K. A. Chen, *Active noise control (Second Edition)*, National Defense Industry Press, 2014.

[26] I. Bruant, L. Gallimard, and S. Nikoukar, "Optimal piezoelectric actuator and sensor location for active vibration control, using genetic algorithm," *Journal of Sound and Vibration*, vol. 329, no. 10, pp. 1615–1635, 2010.

[27] L. Song and P. Xia, "Active control of helicopter structural response using piezoelectric stack actuators," *Journal of Aircraft*, vol. 50, no. 2, pp. 659–663, 2013.

[28] S. D. Snyder and C. H. Hansen, "The effect of transfer function estimation errors on the filtered-x LMS algorithm," *IEEE Transactions on Signal Processing*, vol. 42, no. 4, pp. 950–953, 1994.

[29] K. Lang, P. Xia, and L. Shang, "New algorithm and experiments for helicopter active control of structural response," *Journal of Aircraft*, vol. 59, no. 5, pp. 1152–1161, 2022.

[30] X. Du, W. Tang, Q. Li, and H. Zhang, "Online secondary path modeling method for adaptive active control of structure response," *Aeronautical Science and Technology*, vol. 26, pp. 43–48, 2015.

[31] H. Song, X. Shan, L. Zhang, G. Wang, and J. Fan, "Research on identification and active vibration control of cantilever structure based on NARX neural network," *Mechanical Systems and Signal Processing*, vol. 171, article 108872, 2022.

[32] Y. Pu, H. Zhou, and Z. Meng, "Multi-channel adaptive active vibration control of piezoelectric smart plate with online secondary path modelling using PZT patches," *Mechanical Systems and Signal Processing*, vol. 120, pp. 166–179, 2019.

[33] J. C. Walchko, K. W. Wang, E. William, J. S. Kim, and E. Smith, "Hybrid feedforward-feedback control for active helicopter vibration suppression," *AHS International 63rd Annual Forum - Proceedings - Riding the Wave of New Vertical Flight Technology*, vol. 3, pp. 1757–1773, 2007.

[34] D. H. Kim, T. J. Kim, S. U. Jung, and D. I. Kwak, "Test and simulation of an active vibration control system for helicopter applications," *International Journal of Aeronautical and Space Sciences*, vol. 17, no. 3, pp. 442–453, 2016.

[35] Y. L. Lee, D. H. Kim, J. S. Park, and S. B. Hong, "Vibration reduction simulations of a lift-offset compound helicopter

using two active control techniques," *Aerospace Science and Technology*, vol. 106, article 106181, 2020.

[36] S. Gao, Q. Huang, Z. Gao, Y. Shao, E. Jiang, and X. Zhu, "Active vibration control algorithm using reference signal self-extraction," *Journal of Vibration, Measurement and Diagnosis*, vol. 30, pp. 514–518, 2010.

[37] S. M. Kuo, A. Gupta, and S. Mallu, "Development of adaptive algorithm for active sound quality control," *Journal of Sound and Vibration*, vol. 299, no. 1-2, pp. 12–21, 2007.